Chemical Science

ROYAL SOCIETY OF CHEMISTRY

EDGE ARTICLE

View Article Online
View Journal

Cite this: DOI: 10.1039/d6sc02501c

All publication charges for this article have been paid for by the Royal Society of Chemistry

Zerovalent transition-metal inverse-sandwich complexes of a diborataanthracene dianion

Alexander Gerstner,[ab] Merle Arrowsmith,[ab] Maximilian Dietz,[ab] Cornelius Mihm[ab] and Holger Braunschweig *[ab]

The 9,10-dihydro-9,10-diboraanthracene (9,10-DHDBA) 2,3,6,7,9,10-Me_6-9,10-DHDBA (**2**) reacted with 1 equiv. $[(MeCN)_3Cr(CO)_3]$ to yield the unsymmetrical half-sandwich complex $[(\eta^6\text{-}\mathbf{2})Cr(CO)_3]$ (**2-Cr**), in which the $Cr(CO)_3$ unit binds exclusively to one DHDBA benzo ring. Reactions of **2** with 2 equiv. $[(MeCN)_3M(CO)_3]$ (M = Cr, Mo, W) yielded the centrosymmetric slipped inverse-sandwich complexes $[\{\mu\text{-}(\eta^6,\eta'^6\text{-}\mathbf{2})\}\{M(CO)_3\}_2]$ (**2-M$_2$**), in which each $M(CO)_3$ unit binds to one of the DHDBA benzo rings, one above and one below the DHDBA plane. The twofold reduction of **2** with Li sand afforded the corresponding diborataanthracene (DBA) dianion, isolated as the C_4B_2-bound inverse-sandwich dilithio complex $[\{\mu\text{-}(\eta^6,\eta^6\text{-}\mathbf{2})\}\{Li(thf)_2\}_2]$ (**3**). The latter reacted with 2 equiv. $[(MeCN)_3Cr(CO)_3]$ (M = Cr, Mo) to yield the first stable zerovalent transition-metal inverse-sandwich complexes of a $[9,10\text{-DBA}]^{2-}$ dianion, complexes $[\{\mu\text{-}(\eta^6,\eta^6\text{-}\mathbf{2})\}\{M(CO)_3Li(thf)_3\}_2]$ (**3-M$_2$**). All new compounds were characterised by multinuclear NMR, UV-vis and IR spectroscopy, and their solid-state structures ascertained by single-crystal X-ray diffraction analyses. Furthermore, DFT calculations provide insight into the electronic structure of the 9,10-DHDBA and $[9,10\text{-DBA}]^{2-}$ fused ring systems, as well as metal-(DH)DBA bonding in the chromium complexes **2-Cr**, **2-Cr$_2$** and **3-Cr$_2$**.

Received 26th March 2026
Accepted 13th May 2026

DOI: 10.1039/d6sc02501c

rsc.li/chemical-science

Introduction

More than seven decades after the landmark isolations of ferrocene, $[(\eta^5\text{-}C_5H_5)_2Fe]$, and the first bis(benzene) complex, $[(\eta^6\text{-}C_6H_6)_2Cr]$,[1] sandwich complexes (or metallocenes), in which the metal centre is wedged between two π carbocycles, have become ubiquitous in organometallic chemistry, and are still finding new applications in small-molecule activation,[2] catalysis,[3] materials design,[4] and even pharmaceutical compounds.[5] While sandwich complexes are now known for nearly all the metals of the periodic table, inverse-sandwich complexes, in which the π carbocycle is wedged between two metal centres (Fig. 1), are less well explored. The formation of stable inverse-sandwich complexes requires a particularly electron-rich, often highly reduced π ligand, capable of coordinating one metal centre on each side, such as the 6π-aromatic cyclobutadiene dianion $[C_4H_4]^{2-}$,[6] the 8π-antiaromatic benzene dianion $[C_6H_6]^{2-}$,[7] the 10π-aromatic benzene tetraanion $[C_6H_6]^{4-}$,[8] or the 10π-aromatic cyclooctatetraene (COT) dianion $[C_8H_8]^{2-}$.[9] As metal···arene bonding in these complexes is mostly ionic in nature, the vast majority of inverse-sandwich complexes involve the more Lewis-acidic s- and f-block metals, kinetic stabilisation being provided by bulky ligand spheres shielding the metal centres and the highly reactive reduced arene.[10]

Excluding triple-decker complexes, in which the metal centres are additionally sandwiched by another arene (usually cyclopentadienyl (Cp^-) or $[COT]^{2-}$),[11] and complexes with only partial metal···arene binding, there are only a handful of non-d^0-metal inverse-sandwich complexes. These include some β-diketiminate-stabilised V(I), Nb(III) and Cr(I) complexes (**I**, Fig. 1),[12] two amidinate-chelated Cr(I) derivatives (**II**),[13] and a series of monovalent Cr(I), Mn(I) and Fe(I) terphenyl complexes (**III**),[14] all with neutral benzene or toluene as the η^6,η^6-bridging ligand. Importantly, there are no known solely CO-bearing transition-metal (TM) inverse-sandwich complexes

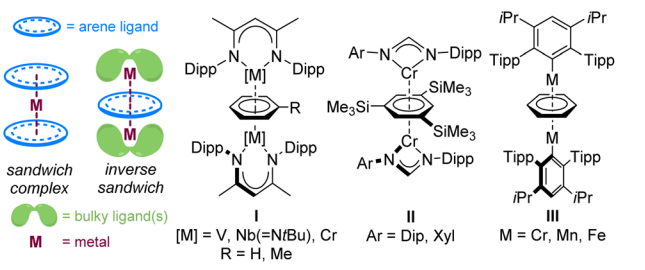

Fig. 1 Examples of known non-d^0 TM inverse-sandwich complexes. Dipp = 2,6-di*iso*propylphenyl; Tipp = 2,4,6-tri*iso*propylphenyl; Xyl = 2,6-dimethylphenyl.

[a]*Institute for Inorganic Chemistry, Julius-Maximilians-Universität Würzburg, Am Hubland, Würzburg 97074, Germany. E-mail: h.braunschweig@uni-wuerzburg.de*
[b]*Institute for Sustainable Chemistry & Catalysis with Boron, Julius-Maximilians-Universität Würzburg, Am Hubland, Germany*

of organic π carbocycles of the form [μ-(η^6,η^6-arene){TM(CO)$_n$}$_2$], as the TM(CO)$_n$ fragments are usually too electron-rich and insufficiently stabilised by the CO ligands.

The replacement of one or more endocyclic CR units by isoelectronic [BL] or [BR]$^-$ units (L = neutral donor, R = anionic substituent) results in a dramatic increase in the electron-donating and π-acceptor ability of the resulting π boracycle compared to its all-carbon analogue, as the incorporation of the electropositive boron atom(s) raises the energy levels of the π-symmetry HOMOs while lowering that of the LUMO.[15] Thus, monoanionic boratabenzenes, [C_5H_5BR]$^-$, although isoelectronic to benzene, are much stronger donors, on a par with the Cp$^-$ ligand,[16] enabling the isolation of a wide array of d- and f-block (half)-sandwich and triple-decker complexes.[17] Whereas benzene only forms sandwich and half-sandwich complexes with Cr(0), Fontaine reported the formation of the Cr(CO)$_3$ boratabenzene inverse-sandwich anion **IV** (Fig. 2) as a byproduct in the synthesis of the piano-stool complex [{η^6-(2-SiMe$_3$-C_5H_4BCl)}Cr(CO)$_3$].[18] Similarly, Herberich showed that a 4π-antiaromatic borole enables the isolation of the Mn(CO)$_3$ inverse-sandwich complex **V**.[19] Finally, borole dianions have been shown to be able to displace isoelectronic Cp$^-$ ligands,[20] thus confirming their stronger donor ability.

The incorporation of two boron atoms into aromatic scaffolds generates even more powerful π ligands. Thus, we have shown that a neutral cyclic alkyl(amino)carbene (CAAC)-stabilised 1,4-diborabenzene (1,4-DBB) ligand is capable of stabilising zerovalent half-sandwich complexes of groups 6 (**VI-M**, M = Cr, Mo, W),[21] 8 (M(CO)$_2$, M = Fe, Ru),[22] and 10 (M(CO), M = Ni).[23] Similarly, neutral diboraacenes like an *N*-heterocyclic carbene (NHC)-stabilised 2,3-diboranaphthalene and a CAAC-stabilised 9,10-diboraanthracene (9,10-DBA) have enabled the isolation of the zerovalent group 6 half-sandwich complexes **VII-M** and **VIII-M** (M = Cr, Mo, W), respectively.[24,25] However, no inverse-sandwich formation has ever been observed with these neutral diboraacenes. Our attention therefore turned to dianionic diboraacenes, which are obtained by the twofold reduction of neutral dihydrodiboraacene precursors,[26] and are known to form sandwich and triple-decker complexes with a small number of d- and f-block metals.[27]

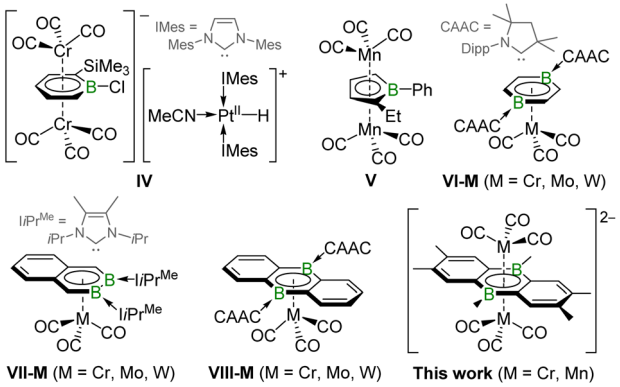

Fig. 2 TM(CO)$_n$ half- and inverse-sandwich complexes of π (di) boracycles.

Herein, we report the synthesis of the mono- and bimetallic zerovalent group 6 complexes of a neutral 9,10-dihydro-9,10-diboraanthracene (9,10-DHDBA) and the first TM inverse-sandwich complexes of its 9,10-diborataanthracene dianion ([9,10-DBA]$^{2-}$).

Results and discussion

Synthesis of (DH)DBA group 6 complexes

The dibromo precursor **1** was synthesised in a manner analogous to its non-methylated analogue[29] by heating a 1 : 2.2 mixture of 1,2-bis(trimethylsilyl)-4,5-dimethylbenzene and BBr_3 in hexane in a sealed thick-walled flask at 120 °C for 3 days (Scheme 1a).† Subsequent methylation with MeMgBr yielded 2,3,6,7,9,10-Me$_6$-9,10-DHDBA (**2**) in near-quantitative yield (Scheme 1b). The ^{11}B NMR shifts in C_6D_6 of **1** and **2** at 62.5 and 67.2 ppm, respectively, as well as their structural parameters (see Fig. S61 and S62 in the SI) are in agreement with those reported for their non-methylated analogues.[28,29] It is noteworthy that in THF, the ^{11}B NMR resonance of compound **2** is upfield-shifted to 58.3 ppm, presumably owing to slow reversible THF coordination to the Lewis-acidic boron centres on the NMR timescale.

The cyclovoltammogram of **2** in THF shows a reversible reduction wave at $E_{1/2} = -2.06$ V and an irreversible one at $E_{pc} = -2.71$ V (see Fig. S61 in the SI). The chemical two-electron reduction of **2** with a large excess of lithium sand in d_8-THF resulted in an instant colour change to pink, then dark red, and the appearance of a new broad ^{11}B NMR resonance at 22.0 ppm, identical to that of the parent [9,10-DBA]$^{2-}$ and the [9,10-Me$_2$-9,10-DBA]$^{2-}$ dilithio complexes (Scheme 1c).[26a,30] The UV-vis spectrum of **3** in THF shows a major absorption at 436 nm with a shoulder at 415 nm, as well as two very broad, low-intensity bands, overlapping in the 500–600 nm region (Fig. 3c). These are slightly red-shifted compared to those of the parent [9,10-DBA][Li(thf)$_2$]$_2$ complex (λ_{max} = 420 nm, λ_2 = 400 nm, λ_3 = 500 nm).[26a] While single crystals of complex **3** suitable for X-ray diffraction analysis could be isolated (see X-ray crystallographic analyses), the compound was not indefinitely stable in the solid state.

The 1 : 1 reaction of [(MeCN)$_3$Cr(CO)$_3$] and **2** in THF at rt led to the formation of the monometallic half–sandwich complex **2-**

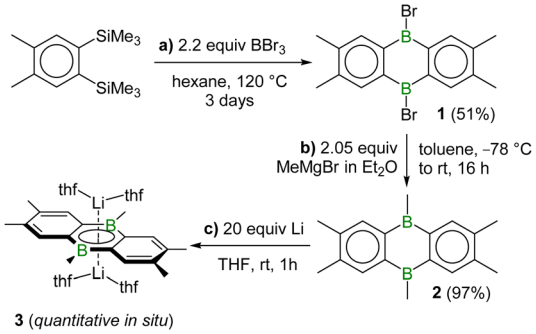

Scheme 1 Synthesis and two-electron-reduction of **2**.

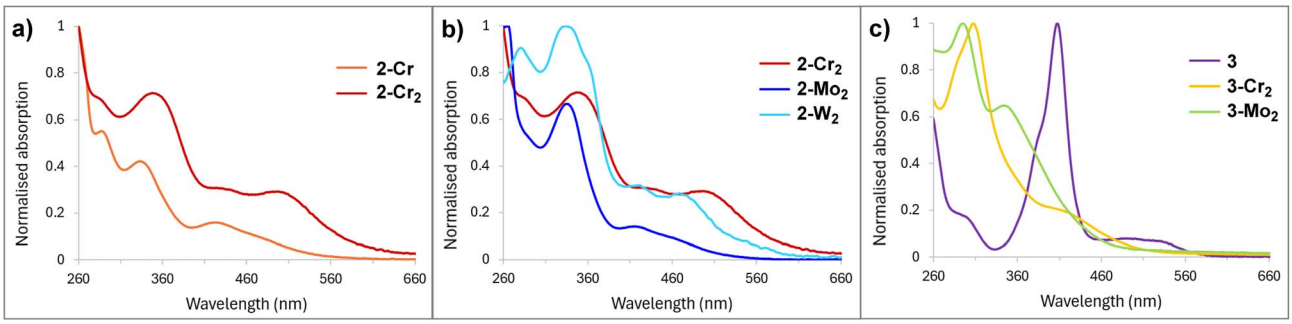

Fig. 3 (a–c) Overlays of the UV-vis spectra of the DHDBA and DBA metal complexes presented herein.

Cr, isolated as a red crystalline solid in 72% yield (Scheme 2a). In d_8-THF the broad ^{11}B NMR resonance of **2-Cr** at 46.3 ppm is significantly upfield-shifted compared to that of **2** ($\delta_{^{11}B}$ = 58.3 ppm). In benzene, however, in which **2-Cr** is only poorly soluble, its ^{11}B NMR resonance shifts back downfield to 64.9 ppm, 6 ppm upfield of the known unsymmetrical Cr(CO)$_3$ complex of 9,10-Me$_2$-9,10-DHDBA ($\delta_{^{11}B}$ = 71 ppm in C_6D_6).[31] The larger upfield-shift of the ^{11}B NMR resonance of **2-Cr** upon switching from benzene to THF ($\Delta\delta \approx -19$ ppm) compared to **2** ($\Delta\delta \approx -9$ ppm) suggests that the boron centres in **2-Cr** bind THF more strongly and are therefore more Lewis-acidic.

In the ^{1}H NMR spectrum, two 2H singlets for the benzo protons, one of which is upfield-shifted to 5.83 ppm due to chromium coordination, reflect the unsymmetrical nature of **2-Cr**. The ^{13}C{^{1}H} NMR spectrum shows a single CO resonance at 234.5 ppm, *ca.* 22 ppm downfield-shifted from those of its 9,10-Me$_2$-DHDBA analogue ($\delta_{^{13}C}$ = 212.8, 212.2 ppm),[31] indicating that the Cr(CO)$_3$ moiety rotates freely in solution. It is noteworthy that the coordination to the 9,10-DHDBA benzo ring is unique to the group 6 metals, as all other low-valent TMs (Fe^0, Ru^0, Co^I, Rh^I, Ni^0, Pd^0, Pt^0) preferentially coordinate to the central 1,4-dibora-2,5-cyclohexadiene ring.[31,32]

The addition of a further equivalent of [(MeCN)$_3$Cr(CO)$_3$] to **2-Cr** yielded the centrosymmetric slipped inverse-sandwich complex **2-Cr$_2$**, isolated as a red crystalline solid in 79% yield (Scheme 2b). The coordination of the second Cr(CO)$_3$ unit results in a small downfield shift of the ^{11}B NMR resonance to 49.1 ppm (THF). A single upfield-shifted benzo singlet (4H) at 5.86 ppm confirms the symmetrical nature of the complex. **2-Cr$_2$** could also be obtained directly from the 2 : 1 reaction of [(MeCN)$_3$Cr(CO)$_3$] and **2** in hexane at 100 °C in a pressurised Schlenk flask (Scheme 2c). Attempted 1 : 1 reactions of the heavier group 6 precursors [(MeCN)$_3$M(CO)$_3$] (M = Mo, W) and **2** did not afford the corresponding mononuclear complexes **2-M** but only a 1 : 1 mixture of bimetallic **2-M$_2$** and unreacted **2**, as determined by NMR spectroscopy. These could be accessed selectively by 2 : 1 reactions in hexane at 100 °C in pressurised Schlenk flasks, yielding **2-Mo$_2$** and **2-W$_2$** as red crystalline solids in moderate yields of 44% and 64%, respectively (Scheme 2c). Both show an ^{11}B NMR resonance around 45 ppm, upfield-shifted from that of **2-Cr$_2$** ($\delta_{^{11}B}$ = 49.1 ppm). The ^{13}C NMR CO resonance of **2-M$_2$** experiences a marked upfield shift upon moving down group 6 ($\delta_{^{13}C}$ = 234.6 (**2-Cr$_2$**), 221.8 (**2-Mo$_2$**), 212.4 (**2-W$_2$**) ppm), with similar chemical shifts to those observed in the [(η^6-mesitylene)M(CO)$_3$] series.[33] The solid-state IR spectra of **2-M$_2$** all display a sharp C=O stretching band around 1936–1944 cm^{-1} and a very broad unresolved band covering the 1800–1875 cm^{-1} range. Both are shifted to slightly lower wavenumbers compared to the parent benzene complexes [(η^6-C$_6$H$_6$)M(CO)$_3$] (ν(C=O)$_{solid-state}$ = 1965–1971, 1845–1875 cm^{-1}),[34] indicating slightly weaker C–O bonds. This suggests that the benzo rings of the 9,10-DHDBA ligand are slightly better overall donors than benzene.

All four 9,10-DHDBA complexes are red. The UV-vis spectra of **2-Cr** and **2-M$_2$** (M = Cr, Mo, W) all show an absorption maximum around λ_{max} = 330–350 nm, as well as two very broad, overlapping, medium-intensity bands in the λ_2 = 415–430 nm and λ_3 = 470–500 nm regions, the latter accounting for their red colour. Comparison of the mono- and bimetallic complexes **2-Cr** (λ = 333, 423, 481 nm) and **2-Cr$_2$** (λ = 349, 431, 497 nm) shows a small redshift for all three bands in the latter (Fig. 3a). Comparison of the three **2-M$_2$** complexes (Fig. 3b), shows a small blueshift upon moving from **2-Cr$_2$** (λ = 349, 431, 497 nm) to **2-Mo$_2$** (λ = 336, 417, 464 nm), and a very minor redshift of λ_2 and λ_3 upon moving from **2-Mo$_2$** to **2-W$_2$** (λ = 334, 422, 469 nm).

Siebert reported that the reduction of his 9,10-Me$_2$-9,10-DHDBA analogue of **2-Cr** with potassium did not lead to the desired shift of the Cr(CO)$_3$ unit to the central C_4B_2 ring but rather to decomposition.[31] We therefore decided to attempt the synthesis of inverse-sandwich complexes starting from the already doubly reduced complex **3**. The addition of 2 equiv. [(MeCN)$_3$Cr(CO)$_3$] (M = Cr, Mo, W) to a freshly prepared THF

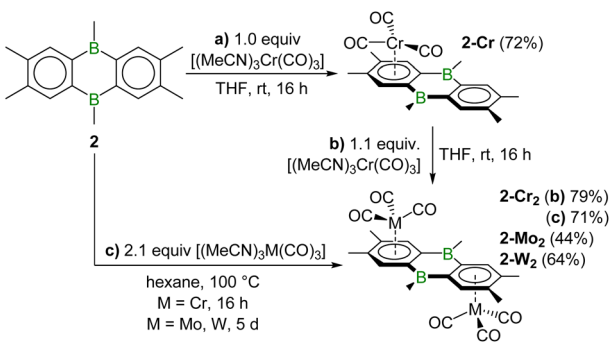

Scheme 2 Synthesis of mono- and bimetallic group 6 complexes of **2**.

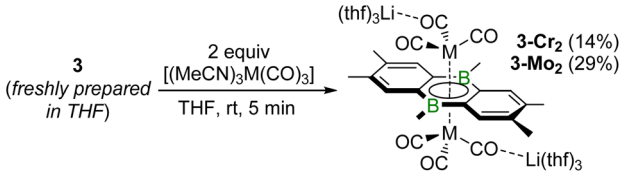

Scheme 3 Synthesis of zerovalent inverse-sandwich group 6 complexes of **3**.

solution of **3** at rt led to the instant formation of dark suspensions. The ^{11}B NMR spectra of the reaction mixture showed the formation of several unidentified sp^3-boron-containing species, as well as a broad resonance at 12 ppm, present in the Cr- and Mo-based reactions, but not in the W-based one. After filtration, removal of the solvent and washing of the solid residues with various solvents, **3-Cr$_2$** and **3-Mo$_2$** were isolated as orange and yellow solids, respectively, in rather poor yields of 14% and 29%, respectively (Scheme 3). It is noteworthy that once formed, **3-Cr$_2$** and **3-Mo$_2$** were indefinitely stable in solution at rt. In the case of the W-based reaction, no equivalent **3-W$_2$** complex was observed, and no other product could be identified. Carrying out the reactions at −78 °C yielded no improvement in their selectivity. To our knowledge, these are the first examples of zerovalent TM inverse-sandwich complexes of a diborataanthracene ligand. The only other known [9,10-DBA]$^{2-}$ complexes beyond the alkali metals are the dilanthanide triple-decker complexes recently reported by Morena-Pineda and Roesky.[27b]

The ^{11}B NMR resonance of **3-Cr$_2$** and **3-Mo$_2$** at *ca.* 12 ppm is 10 ppm upfield-shifted compared to **3** ($\delta_{^{11}B}$ = 22 ppm), indicating a significant increase in electron density at the boron centres from interaction with the electron-rich Cr(0) centres (see DFT calculations). The centrosymmetric nature of **3-M$_2$** was attested by the single ^{1}H NMR benzo singlet (4H) at 7.45 ppm. In solution the Cr(CO)$_3$ units rotate freely and the [Li(thf)$_3$]$^+$ units fluctuate between all three CO ligands on the NMR timescale, as only one ^{13}C NMR carbonyl resonance is observed ($\delta_{^{11}C}$ = 242.0 (**3-Cr$_2$**), 234.6 (**3-Mo$_2$**) ppm). The solid-state IR spectra reflect the presence of the Li-bound CO ligands through a series of stretching bands spanning the 1711–1935 cm^{-1} region, with the bands above 1850 cm^{-1} pertaining to the terminal CO ligands and those below 1800 cm^{-1} to those of the weaker Li-bound C=O bonds. As expected from the differences in colour, the UV-vis spectra of **3-M$_2$** (M = Cr, orange; M = Mo, yellow) differ greatly from that of their precursor **3** (red). Thus, **3-M$_2$** show only low-intensity absorptions around 440 nm, where **3** displays its λ_{max}, and lack any bands in the 500–600 nm region (Fig. 3c). Both their absorption maxima (**3-Cr$_2$** λ = 308, 418 nm; **3-Mo$_2$** λ = 296, 344 nm) are significantly blueshifted from those of **2-M$_2$**. Furthermore, a blueshift is observed upon moving from **3-Cr$_2$** to the heavier **3-Mo$_2$**, as already noted between **2-Cr$_2$** and **2-Mo$_2$**.

Table 1 ^{11}B NMR shifts (ppm) in d$_8$-THF, and selected bond distances (Å) and torsion angles (°) of the crystallographically characterised compounds presented herein $\overline{a/a'}, \overline{b/b'}, \overline{c/c'}, \overline{d/d'}, \overline{e/e'}$ = avg. edge length (see edge labels below); $\overline{M\cdots DBA}$ = avg. distance between the metal centre and the mean plane of the ring it coordinates to; $\overline{M\text{–}C_{d/e}}$ = avg. distance between the metal centre and the carbon atoms of the *e*/*e*′ (and *d*/*d*′) edges of the ring it coordinates to; $\overline{M\text{–}CO}$ = avg. metal – carbonyl bond lengths; $\overline{C\text{–}O}$ = avg. carbonyl C–O bond lengths; $|\omega_{max}|$ = absolute value of the largest endocyclic torsion angle of the central B_2C_4 ring; φ = angle between the mean planes of the benzo and C_4B_2 rings

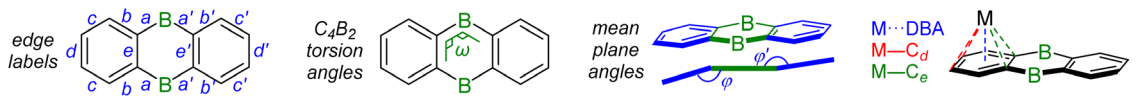

	^{11}B NMR	$\overline{a/a'}$	$\overline{e/e'}$	$\overline{b/b'}$	$\overline{c/c'}$	$\overline{d/d'}$	$\overline{M\cdots DBA}$	$\overline{M\text{–}C_{d/e}}$	$\overline{M\text{–}CO}$	$\overline{C\text{–}O}$	$\lvert\omega_{max}\rvert$	φ/φ'
2	58.3	1.565(2)	1.419(2)	1.404(2)	1.395(2)	1.401(2)	—	—	—	—	10.6(2)	*ca.* 4.0
3	22.0	1.531(3)	1.472(3)	1.438(3)	1.370(3)	1.441(3)	*ca.* 1.87	2.385(4)[c]	—	—	1.1(3)	*ca.* 0.9
2-Cr	46.3	1.573(4)[a]	1.433(4)[a]	1.434(4)[a]	1.406(4)[a]	1.427(4)[a]	*ca.* 1.72	2.193(3)[c]	1.847(3)	1.156(4)	8.4(4)	*ca.* 5.2[a]
		1.557(4)[b]	1.421(4)[b]	1.400(4)[b]	1.396(4)[b]	1.392(4)[b]		2.263(3)[d]				*ca.* 5.0[b]
2-Cr$_2$	49.1	1.559(3)	1.451(3)	1.415(3)	1.421(3)	1.405(3)	*ca.* 1.71	2.201(2)[c]	1.853(3)	1.151(3)	2.5(3)	*ca.* 9.3
								2.263(2)[d]				
2-Mo$_2$	45.0	1.562(4)	1.450(4)	1.428(4)	1.403(4)	1.434(4)	*ca.* 1.88	2.316(3)[c]	1.984(3)	1.147(4)	6.3(4)	*ca.* 9.4
								2.400(3)[d]				
2-W$_2$	44.4	1.560(7)	1.444(6)	1.425(7)	1.415(7)	1.423(7)	*ca.* 1.87	2.311(2)[c]	1.964(7)	1.144(9)	8.9(6)	*ca.* 11.8
								2.390(6)[d]				
3-Cr$_2$[e]	11.9	1.551(3)	1.457(2)	1.449(3)	1.355(3)	1.449(2)	*ca.* 1.78	2.287(2)	1.816(2)[g]	1.173(3)[g]	2.0(2)	*ca.* 2.3
								2.369(2)[f]	1.779(2)[h]	1.191(3)[h]		*ca.* 0.8[f]
3-Mo$_2$[e]	12.0	1.557(9)	1.463(8)	1.448(9)	1.357(9)	1.443(9)	*ca.* 1.95	2.424(6)	1.931(7)[g]	1.173(9)[g]	1.6(8)	*ca.* 2.2
								2.500(6)[f]	1.889(10)[h]	1.197(10)[h]		*ca.* 0.7[f]

[a] Within the metal-containing complex moiety. [b] within the metal-free complex moiety. [c] $\overline{M\text{–}C_{e/e'}}$. [d] $\overline{M\text{–}C_{d/d'}}$. [e] values provided for both molecules present in the asymmetric unit. [f] different avg. values measured for the *e* and *e*′ edge. [g] for terminal CO ligands. [h] for Li-bound CO ligands.

X-ray crystallographic analyses

Compound 2. The central 1,4-dibora-2,5-cyclohexadiene ring of **2** is slightly bent along the B···B axis (*ca.* 7.8°, see Fig. S63 in the SI). The endocyclic B–C bond lengths (avg. 1.565(2) Å) are typical for single bonds at sp^2-hybridised boron. The C–C bonds of the outer *b*, *c* and *d* edges (see edges labelling in Table 1) show a relatively low degree of bond alternation (1.393(2)–1.406(2) Å), with the ring junctions *e* being slightly elongated (1.419(2) Å), indicating good π delocalisation over the benzo rings (see DFT calculations). Overall, these structural parameters are similar to those of the analogous 9,10-Me_2-9,10-DHDBA.[29]

Complexes 2-M_n. Complexes **2-Cr** and **2-M_2** (M = Cr, Mo, W) all provided red single crystals suitable for SCXRD analyses. The solid-state structure of **2-Cr** shows a single $Cr(CO)_3$ fragment η^6-coordinated to one of the benzo rings (Cr···C_6 1.72 Å, Fig. 4, Table 1). In a similar manner, $Cr(CO)_3$ also coordinates to the outer ring of anthracene.[35] Metal coordination results in a small but significant (*ca.* 0.04 Å) lengthening of the *b* and *d* edges compared to the uncoordinated benzo ring. It is noteworthy that the $Cr(CO)_3$ is not centrally positioned above the benzo ring, but somewhat closer to the *e* than to the *d* edge (avg. Cr–C_e 2.193(3) Å; avg. Cr–C_d 2.263(3) Å, see explanation in DFT calculations). The $Cr(CO)_3$ fragment is staggered with respect to the benzo ring, one CO ligand pointing towards the *d* edge. The Cr–C_{CO} (1.843(3)–1.849(3) Å) and C–O (1.153(4)–1.157(4) Å) bond lengths show less variation than in the isostructural [(η^6-anthracene)$Cr(CO)_3$] complex (Cr–C 1.812(10)–1.834(10) Å; C–O (1.142(10)–1.184(12) Å).[35]

In contrast to **2-Cr**, the three bimetallic complexes **2-M_2** are centrosymmetric, with one $M(CO)_3$ fragment η^6-coordinated to each benzo ring, one above and one below the 9,10-DHDBA plane, in what may be called a slipped inverse-sandwich coordination mode (Fig. 4 and Table 1, see Fig. S68 in the SI for **2-W_2**). Whereas the central C_4B_2 ring in **2-Cr_2** is virtually planar ($|\omega_{max}|$ = 2.5(3)°), it is slightly twisted in the two heavier analogues (**2-Mo_2** 6.3(4)°, **2-W_2** 8.9(6)°). Furthermore, all three complexes display a significant bend in the overall 9,10-DHDBA framework, the angle φ formed by the C_6 and C_4B_2 mean planes ranging from 9.3° to 11.8°. The endocyclic C–C and B–C bond lengths of all three dinuclear complexes are similar within the error of the measurement. The M···C_6 distance increases significantly from **2-Cr_2** (*ca.* 1.71 Å) to **2-Mo_2** (*ca.* 1.88 Å) but shows no further increase for **2-W_2** (*ca.* 1.87 Å). This is in line with the much lower difference between the hexacoordinate metallic radii of W and Mo, than of Mo and Cr (Cr 1.285, Mo 1.402, W 1.410 Å),[36] owed to the f-orbital contraction in W. These M···C_6 distances are all slightly shorter than those found in the [(η^6-C_6H_6)$M(CO)_3$] series (Cr 1.72, Mo 1.91, W 1.90 Å),[37] suggesting stronger metal···arene bonding. Complexes **2-M_2** display the same slightly unsymmetrical positioning of the metal centres above the C_6 rings as **2-Cr**, the M–C_d bonds being *ca.* 3% longer than the M–C_e bonds, owing to the influence of the fused electron-poor C_4B_2 ring (see DFT calculations). Whereas the $M(CO)_3$ fragments in **2-Cr_2** are staggered with respect to the benzo rings, this time with one CO ligand each pointing towards the central C_4B_2 ring, those in **2-Mo_2** and **2-W_2** are nearly eclipsed. These conformational differences may be at the origin of the differing degrees of distortion from planarity observed in their C_4B_2 rings (*vide supra*). Finally, the C–O bond lengths of all three complexes are statistically similar, in line with their very similar IR C–O stretching bands (*vide supra*).

Complex 3. While complex **3** was too sensitive to be isolated in bulk, recrystallisation by diffusion of hexane into a saturated

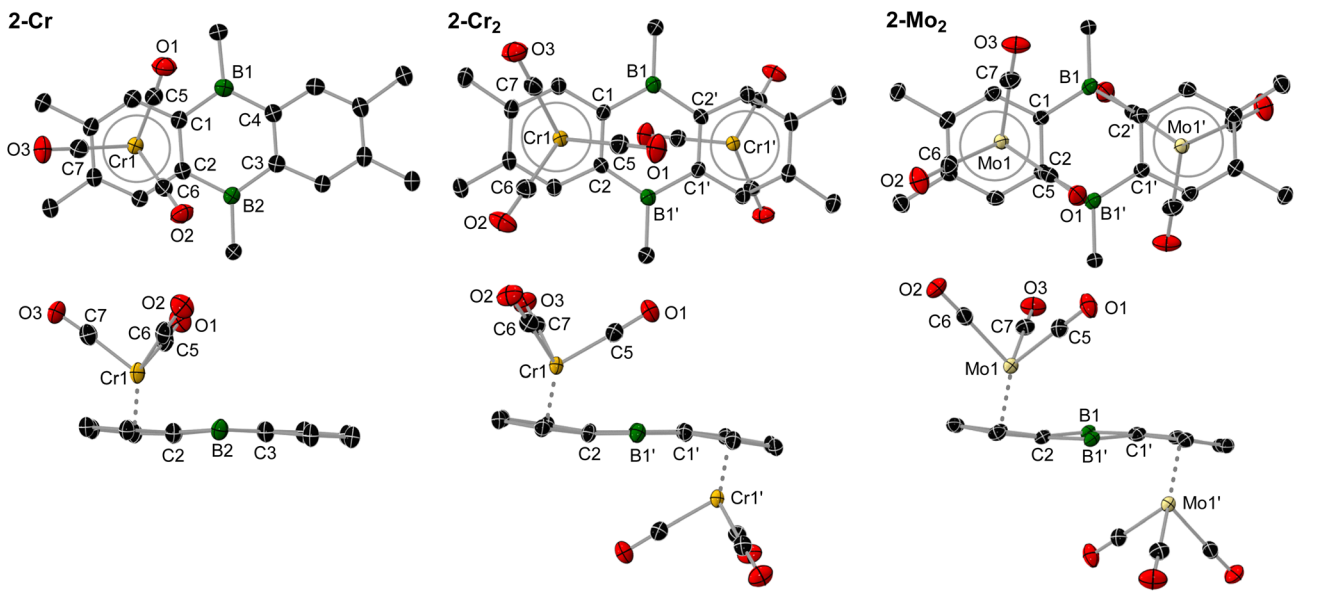

Fig. 4 Crystallographically determined solid-state structures of **2-Cr**, **2-Cr_2** and **2-Mo_2**. Top: views from above the DHDBA plane, highlighting the various conformations of the $M(CO)_3$ moieties with respect to the DHDBA framework and to each other. Below: truncated views (methyl groups omitted) along the B···B axis, highlighting the bend in the DHDBA framework. Thermal displacement ellipsoids set at 50% probability. Hydrogen atoms omitted for clarity.

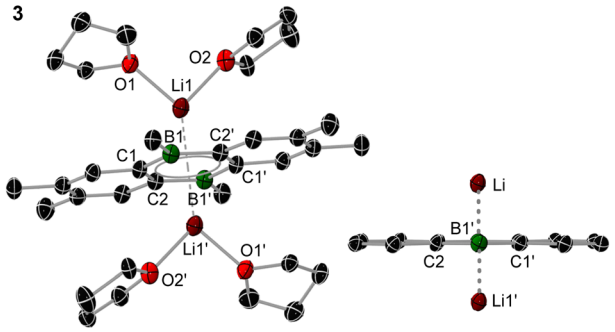

Fig. 5 Left: crystallographically determined solid-state structure of **3**. Right: truncated view of **3** (methyl groups and THF ligands omitted) along the B···B axis, highlighting the planarity of the DBA framework. Thermal displacement ellipsoids set at 50% probability. Hydrogen atoms omitted for clarity.

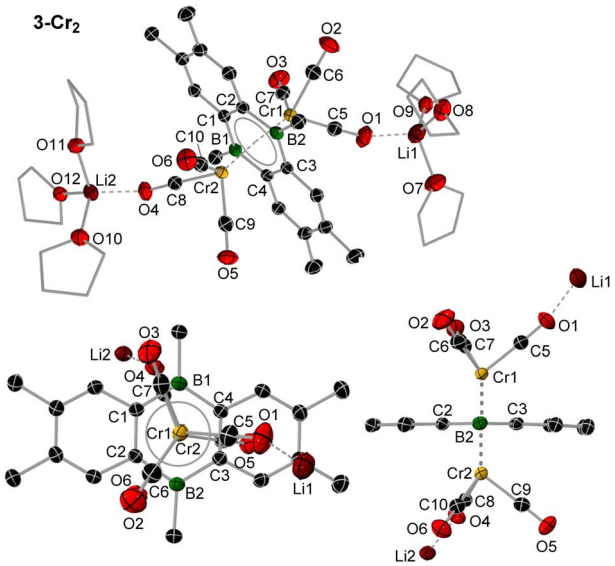

Fig. 6 Top: crystallographically determined solid-state structure of **3-Cr$_2$**. Bottom left: view of **3-Cr$_2$** (THF ligands omitted) from above the DBA plane, highlighting the eclipsed conformation of the Cr(CO)$_3$ moieties. Bottom right: truncated view of **3-Cr$_2$** along the B···B axis (methyl groups and THF omitted), highlighting the planarity of the DBA framework. Thermal displacement ellipsoids set at 50% probability. Hydrogen atoms omitted for clarity.

THF solution at −30 °C yielded red crystals suitable for SCXRD analysis. The solid-state structure of **3** is centrosymmetric and shows an inverse-sandwich complex, with the lithium cations sitting atop and below the centre of the central B_2C_4 ring (Li···B_2C_4 *ca.* 1.87 Å), each coordinated by two THF molecules (Fig. 5 and Table 1). The aromatisation of the B_2C_4 ring is seen in the shortening of its endocyclic B–C bonds (**3** 1.531(3); **2** 1.565(2) Å), the substantial lengthening of its C–C bonds (**3** 1.472(3); **2** 1.419(2) Å), and its higher degree of planarity compared to **2** ($|\omega_{max}|$: **3** 1.1(3); **2** 10.6(2)°). Conversely, the fused benzo rings become less aromatic, now approaching alternating C–C single (1.438(3), 1.441(3) Å) and double (1.370(3) Å) bonds. Furthermore, the entire DBA framework is now virtually planar ($\varphi < 1°$). These bonding parameters are similar to those found in other inverse-sandwich [9,10-DBA]Li$_2$ complexes.[26a,38]

Complexes 3-M$_2$. **3-Cr$_2$** and **3-Mo$_2$** are isomorphous, crystallising in the $P2_1/c$ space group with near-identical cell parameters ($a \approx 42.0$ Å, $b \approx 10.4$ Å, $c \approx 24.0$ Å, $\beta = 105°$). Their asymmetric units contain two crystallographically distinct molecules of **3-M$_2$**. In each, two M(CO)$_3$ fragments are η^6-bound to the central 1,4-DBB ring, while the Li(thf)$_3$ cations coordinate to one of their CO ligands *via* Li–O linkages (Fig. 6 and Table 1, for **3-Mo$_2$** see Fig. S70 in the SI. Similarly to **3**, the entire [9,10-DBA]$^{2-}$ framework is quasi-planar ($|\omega_{max}| \leq 2.3(9)°$, $\varphi \leq 2.2°$). The endocyclic B–C and C–C bond lengths in **3-Cr$_2$**, **3-Mo$_2$** are similar within the error of the measurements. Compared to the related neutral diboraacene complexes **VI-M** and **VIII-M**,[21,25] or Roesky's [9,10-DBA]Ln$_2$ triple-decker complexes,[27b] the endocyclic B–C bond lengths in **3-M$_2$** are slightly longer (*ca.* 1.55 *vs.* 1.53 Å), suggesting a slightly lower degree of π conjugation within the C_4B_2 ring. The Cr···C_4B_2 distances in **3-M$_2$** (**3-Cr$_2$** *ca.* 1.78 Å, **3-Mo$_2$** *ca.* 1.95 Å) are shorter than in the corresponding neutral half-sandwich complexes **VIII-M** (*ca.* 1.80 Å). In both complexes, the M(CO)$_3$ units are staggered with respect to the C_4B_2 rings but eclipsed with respect to each other. One of the Li$^+$ cations coordinates to a CO pointing across one *a* edge, while the other links to the CO pointing across the *e* edge, creating an asymmetry between the two sides of the DBA framework. This results in the two metal centres being shifted slightly off-centre, *ca.* 3% closer to C3–C4 than to the C1–C2 bond. Whereas the terminal CO ligands all show similar C–O bond lengths (avg. 1.173(9) Å), the Li-bound ones are slightly elongated (avg. 1.194(10) Å), resulting in the lower wavenumber set of stretching bands observed in the solid-state IR spectra (*vide supra*).

DFT calculations

Compounds 2 and its dianion. In order to quantify the aromaticity changes upon twofold reduction of **2**, nucleus-independent chemical shift (NICS)[39] calculations were carried out at the B3LYP-D4-def2-SVP level of theory on the structures of **2** and its naked dianion **[2]$^{2-}$** (without the Li(thf)$_2$ moieties) optimised at the ωB97X-D4-def2-SVP level of theory (see details in the SI). Benzene, with a highly negative NICS(±1)$_{zz}$ value of −29.1 ppm was used as a reference (Table 2).

For the two benzo rings the aromaticity decreases slightly upon reduction to the dianion, as seen in their slightly less negative NICS(±1)$_{zz}$ value (**2** −20.5 ppm; **[2]$^{2-}$** −17.5 ppm). In contrast, the central C_4B_2 ring switches from antiaromatic in **2**, with an average positive NICS(±1)$_{zz}$ value of +16.6 ppm, to highly aromatic in **[2]$^{2-}$**, with a NICS(±1)$_{zz}$ value of −32.3 ppm, more negative than that of benzene. It is noteworthy that in compound **2** the substantial difference between the NICS(−1)$_{zz}$ (19.7 ppm) and NICS(+1)$_{zz}$ (13.0 ppm) values of the C_4B_2 ring is owed to its slightly bent geometry (see X-ray crystallographic analyses). For **[2]$^{2-}$** the NICS(−1)$_{zz}$ and NICS(+1)$_{zz}$ values are identical within the error of the calculation, in line with the planarisation of the C_4B_2 ring upon twofold reduction. For comparison, the central ring of the literature-known [9,10-Mes$_2$-9,10-DBA]$^{2-}$ dianion (Mes = 2,4,6-trimethylphenyl), for which only the NICS(0) and NICS(1) values are reported, (−9.0/−13.1

Table 2 NICS(0), NICS(1) and NICS(±1)$_{zz}$ (average of NICS(1)$_{zz}$ and NICS(−1)$_{zz}$) values (ppm) and C–C/C–B WBIs calculated at the B3LYP-D4-def2-SVP//ωB97X-D4-def2-SVP level of theory

	C_4B_2 ring				C_6 rings				
	NICS		WBI		NICS		WBI		
	(0/1)	$(\pm1)_{zz}$	*a*	*e*	(0/1)	$(\pm1)_{zz}$	*b*	*c*	*d*
C_6H_6	—	—	—	—	−8.9/−11.0	−29.1		1.41	
2	10.3/2.4	19.7, 13.0[a]	1.06	1.33	−4.8/−8.8	−20.5	1.33	1.39	1.39
$[\mathbf{2}]^{2-}$	−8.2/−11.4	−32.2	1.33	1.21	−4.6/−7.4	−17.5	1.16	1.53	1.20

[a] The slight bend in the C_4B_2 ring results in different NICS(1)$_{zz}$ and NICS(−1)$_{zz}$ values.

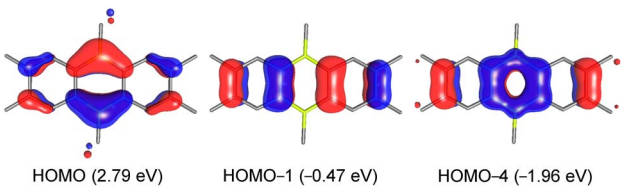

Fig. 7 Plots of the frontier MOs of $[\mathbf{2}]^{2-}$ involving π delocalisation over the C_4B_2 ring, energy levels in parentheses. Isovalues: 0.04.

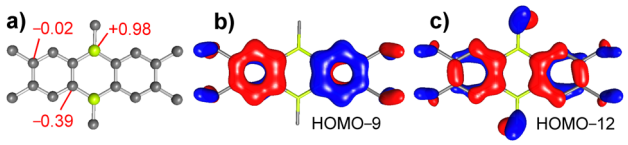

Fig. 8 (a) Optimised structure of **2** at the ωB97X-D4-def2-SVP level of theory, with NBO charges of the *d* and *e* carbon and boron atoms in red. Atom colours: carbon = grey, boron = green. Hydrogen atoms omitted for clarity. (b and c) Plots of the HOMO−9 and HOMO−12 of **2**. Isovalues: 0.04.

ppm),[40] is slightly more aromatic than that of $[\mathbf{2}]^{2-}$ (−8.2/−11.4 ppm). Moreover, the aromatisation of the C_4B_2 ring is also visible in its B–C Wiberg bond indices (WBIs), which increase from 1.06 in **2** (single bonds) to 1.33 in $[\mathbf{2}]^{2-}$ (partial double bonds), concomitant with a slight decrease in its C–C WBIs, from 1.33 to 1.21, respectively (Table 2).[41] At the same time the benzo rings lose some of their aromatic character, as seen in the wider range of C–C WBIs ($[\mathbf{2}]^{2-}$ 1.16–1.53, **2** 1.33–1.39).

The aromatisation of the C_4B_2 ring is also apparent in the frontier MOs. Whereas the π-symmetry HOMOs of **2** are all delocalised over the two benzo rings, the HOMO (which corresponds to the LUMO of **2**), HOMO−1, and HOMO−4 of $[\mathbf{2}]^{2-}$ show π delocalisation over the 1,4-diboratabenzene ring akin to that of benzene (Fig. 7).

Compounds 2-Cr and 2-Cr$_2$. Attempts to optimise **2-Cr** and **2-Cr$_2$** to the geometries observed in the solid state revealed that the various orientations of the Cr(CO)$_3$ unit(s) with respect to 9,10-DHDBA framework are very close in energy (<1 kcal mol^{-1}) and display very low rotation barriers (<1 kcal mol^{-1}, see Fig. S75 in the SI). This explains the variety of conformations observed for **2-Cr** and **2-M$_2$** (M = Cr, Mo, W) in the SCXRD-derived solid-state structures (Fig. 4). Furthermore, calculations show that the putative η^6-C_4B_2 isomer of **2-Cr**, complex **2′-Cr** (see Fig. S72 in the SI), is 22 kcal mol^{-1} higher in energy than **2-Cr**, thus reflecting the exclusive preference of Cr for η^6-benzo complexation.

The optimised structures of **2-Cr** and **2-Cr$_2$** in the solid-state conformations reproduce the slightly off-centre position of the Cr atoms, which are closer to the *e* than *d* edge(s) (Cr–C$_d$ 2.229, Cr–C$_e$ 2.184 Å). A look at the natural bond orbital (NBO)[42] charges of the benzo rings of **2** (Fig. 8a) shows that the *e*-edge carbon atoms are significantly more negative (−0.39) than the *d*-edge ones (−0.02) due to the polarisation of the benzo π electron density towards the electron-deficient boron atoms (+0.98) of the central ring. This polarisation is also visible in the unsymmetrical π-electron distribution of the HOMO−9 and HOMO−12 (Fig. 8b and c), resulting in tighter binding of the Cr centres to the *e* edges in **2-Cr** and **2-Cr$_2$**.

Compound 3-Cr$_2$. The optimised structure of compound **3-Cr$_2$** starting from the SCXRD-derived solid-state structure reproduces the staggered conformation of the Cr(CO)$_3$ units with respect to the C_4B_2 ring and their eclipsed conformation with respect to each other, as well as the binding of the Li$^+$ cations to CO ligands pointing in different directions, and the unsymmetrical positioning of the Cr centres closer to the *e* edges over which the C5–O1···Li1(thf)$_3$ and C9–O5 carbonyl ligands point. This asymmetry is also visible in the frontier MOs of this structure (see Fig. S74 in the SI). However, since this asymmetry is only present in the solid state, while in solution the Cr(CO)$_3$ moieties rotate freely and the [Li(thf)$_3$]$^+$ cations fluctuate between all three CO ligands, further calculations were carried out on the dianionic part of **3-Cr$_2$** ($[\mathbf{3'\text{-}Cr_2}]^{2-}$) only. Optimisation of several possible conformations of $[\mathbf{3'\text{-}Cr_2}]^{2-}$ show that that of the solid-state conformation of $[\mathbf{3'\text{-}Cr_2}]^{2-}$ is the overall minimum. The HOMO and HOMO−2 to HOMO−5 of $[\mathbf{3'\text{-}Cr_2}]^{2-}$ are entirely Cr(CO)$_3$-based, while HOMO−6 to HOMO−10, HOMO−16 and HOMO−18 essentially correspond to the π-delocalised orbitals of the anion $[\mathbf{2}]^{2-}$, each with very small σ-bonding contributions to the matching chromium d orbitals. Only the HOMO−1 and HOMO−6 present significant σ bonding between the chromium d orbitals and the B–C π bonds of one half of the C_4B_2 ring, respectively (Fig. 9).

An intrinsic bonding orbital (IBO)[43] analysis shows three IBOs involved in Cr···C_4B_2 bonding (Fig. 10). IBO-1 and IBO-2

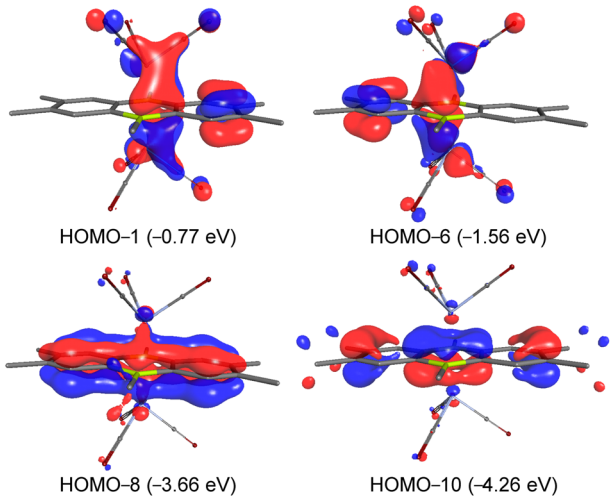

Fig. 9 Plots of the frontier MOs of $[\mathbf{3'\text{-}Cr_2}]^{2-}$ involved in Cr···C_4B_2 bonding. Energy levels in parentheses. Isovalues: 0.04.

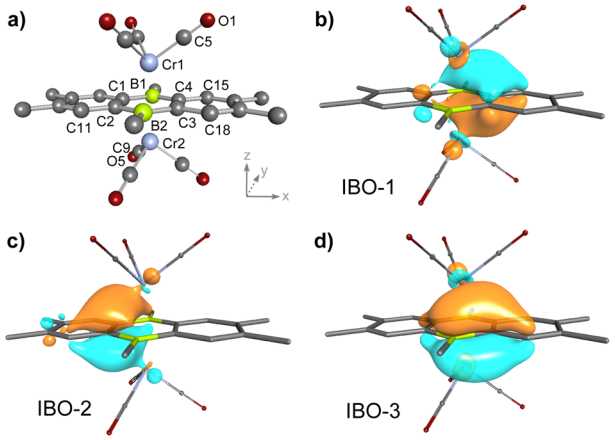

Fig. 10 (a) Optimised structure of $[\mathbf{3'\text{-}Cr_2}]^{2-}$ at the ωB97X-D4-def2-SVP level of theory. The hydrogen atoms and Li(thf)$_3$ moieties have been omitted for clarity. (b–d) IBOs of $[\mathbf{3'\text{-}Cr_2}]^{2-}$ involved in Cr···C_4B_2 bonding. Main orbital contributions to IBO-1: 21% $2p_z$(B1), 47% $2p_z$(C4), 4% $2p_z$(C15), 4% $2p_z$(C3), 2% $2p_z$(C2), 3% $3d_{xz}$(Cr2), 2% $3d_{xz}$(Cr1); to IBO-2: 4% $2p_z$(B1), 40% $2p_z$(C1), 35% $2p_z$(C2), 2% $2p_z$(B2), 1% $3d_{xz}$(Cr1), 1% $3d_{xz}$(Cr2); to IBO-3: 2% $2p_z$(C2), 22% $2p_z$(B2), 46% $2p_z$(C3), 3% $2p_z$(C18), 3% $2p_z$(C4), 4% $3d_{yz}$(Cr1), 4% $3d_{yz}$(Cr2). Isovalues: 0.04.

involve σ donation from essentially the B1–C4 (68% contribution) and C1–C2 (75%) π bonds into the two chromium d_{xz} orbitals (6%, respectively), while IBO-3 involves donation from the B2–C3 π bond (68%) into the chromium d_{yz} orbitals (8%). It is noteworthy that the contribution of each boron $2p_z$ orbital to these three IBOs (*ca.* 24%) is significantly lower than that of each carbon one (*ca.* 40% for C1/C2, *ca.* 50% for C3/C4). The rather low chromium contributions (≤4% per Cr) to these IBOs suggest that the $Cr^0 \leftarrow [\mathbf{2}]^{2-} \rightarrow Cr^0$ interaction is mainly electrostatic in nature. Interestingly, an atoms-in-molecules (AIM)[44] analysis provides bond critical points (BCP) only for the Cr–C bonds, and none for the Cr···B interactions (see Fig. S76 in the SI).

Conclusions

We have shown that the neutral 9,10-DHDBA **2** and its doubly reduced $[9,10\text{-DBA}]^{2-}$ dilithio inverse-sandwich complex **3** are suitable precursors for the complexation of group 6 carbonyls. While compound **2** forms a stable, unsymmetrical half-sandwich complex (**2-Cr**) by coordination of $Cr(CO)_3$ to one of the benzo rings, the analogous Mo and W complexes are not accessible. DFT calculations show that coordination to the central C_4B_2 ring is disfavoured by 22 kcal mol^{-1}. In contrast, all three group 6 metals form stable centrosymmetric slipped inverse-sandwich complexes (**2-M$_2$**, M = Cr, Mo, W) by coordination of one $M(CO)_3$ to each benzo ring, one above and one below the DHDBA plane. These all display a slightly bent DHDBA framework, with the metal centres coordinating more tightly to the ring junctions, where π density accumulates due to the attraction exerted by the central electrophilic boron atoms.

Twofold reduction of **2** with lithium yields the inverse-sandwich complex **3**, in which the two lithium cations coordinate to either side of the now aromatic central 1,4-diborabenzene ring. While **3** is only stable in solution, its reaction with $[M(CO)_3(NCMe)_3]$ (M = Cr, Mo) yielded the first stable zerovalent TM inverse-sandwich complexes of a diborataanthracene ligand (**3-M$_2$**, M = Cr, Mo), albeit in poor yields. SCXRD analyses confirm that the two $M(CO)_3$ units bind in an η^6 fashion to the central C_4B_2 ring of the DBA dianion, while the $[Li(thf)_3]^+$ countercations bind to one CO ligand of each $M(CO)_3$ unit. Finally, DFT calculations show that $M(CO)_3$ bonding to the central 1,4-diborabenzene ring in **3-M$_2$** is mainly electrostatic in nature, without formal Cr–B bonding.

Author contributions

AG designed the study, conducted the experimental work and data analysis, and wrote the SI. MA carried out computations and wrote the manuscript. AG, MD and CM carried out SCXRD experiments and refined the data. HB conceived the project, and provided funding and supervision. All authors were involved in the finalisation of manuscript and SI.

Conflicts of interest

There are no conflicts to declare.

Data availability

CCDC 2538786, 2538787, 2538788, 2538789, 2538790, 2538791, 2538792, 2538793 and 2538794 contain the supplementary crystallographic data for this paper.[45a–i]

The data supporting the findings are included in the supplementary information (SI). Supplementary information: synthetic procedures, NMR, IR, and UV-vis spectra, cyclovoltamograms, X-ray crystallographic and computational details, Cartesian coordinates of calculated structures. See DOI: https://doi.org/10.1039/d6sc02501c.

Acknowledgements

The authors gratefully acknowledge funding from the Deutsche Forschungsgesellschaft (DFG grants BR1149/30-1 466754611) and a Fonds der Chemischen Industrie (FCI) Kékulé stipend for AG.

Notes and references

† There is one important difference: whereas 9,10-Br_2-9,10-DHDBA only forms under static reduced pressure (*i.e.* evacuation of the headspace of the flask prior to heating), **1** only forms under elevated pressure. Under static reduced pressure, the reaction yields 1,2-bis(dibromoboryl)-4,5-dimethylbenzene instead.

1 (*a*) T. J. Kealy and P. L. Pauson, *Nature*, 1951, **168**, 1039–1040; (*b*) E. O. Fischer and W. U. Hafner, *Z. Naturforsch., B*, 1955, **10**, 665–668.

2 (*a*) U. Rosenthal, *Angew. Chem., Int. Ed.*, 2018, **57**, 14718–14735; (*b*) L. Becker and U. Rosenthal, *Coord. Chem. Rev.*, 2017, **345**, 137–149; (*c*) S. Schäfer, S. Kaufmann, E. S. Rösch and P. W. Roesky, *Chem. Soc. Rev.*, 2023, **52**, 4006–4045; (*d*) P. J. Chirik, *Organometallics*, 2010, **29**, 1500–1517.

3 (*a*) A. Desgranges, F. D'Agosto and C. Boisson, *ChemPlusChem*, 2024, **89**, e202400262; (*b*) J. Okuda, *J. Organomet. Chem.*, 2023, 1000; (*c*) H. G. Alt, Metallocene Complexes as Catalysts for Olefin Polymerization, *Coord. Chem. Rev.*, 2006, **250**, 1–272.

4 (*a*) T. Wang and D. Astruc, *Coord. Chem. Rev.*, 2025, **524**, 216300; (*b*) M. V. Kharlamova and C. Kramberger, *Nanomat*, 2023, **13**, 774; (*c*) A. Zabala-Lekuona, J. M. Seco and E. Colacio, *Coord. Chem. Rev.*, 2021, **441**, 213984; (*d*) H. Gu, R. Ciganda, S. Gatard, F. Lu, P. Zhao, J. Ruiz and D. Astruc, *J. Organomet. Chem.*, 2016, **821**, 54–61; (*e*) D. Astruc, C. Ornelas and J. Ruiz, *Chem. Eur J.*, 2009, **15**, 8936–8944.

5 (*a*) A. Kalamatianou, C. Ludwig, S. Zhong, K. Cariou and G. Gasser, *Chem. Soc. Rev.*, 2025, **54**, 3930–3961; (*b*) I. Kostova, *Molecules*, 2024, **29**, 824; (*c*) M. M. Santos, P. Bastos, I. Catela, K. Zalewska and L. C. Branco, *Mini-Rev. Med. Chem.*, 2017, **17**, 771–784.

6 (*a*) D. Patel, J. McMaster, W. Lewis, A. J. Blake and S. T. Liddle, *Nat. Commun.*, 2013, **4**, 2323; (*b*) C. Yu, B. Wu, Z. Yang, H. Chen, W.-X. Zhang and Z. Xi, *Bull. Chem. Soc. Jpn.*, 2020, **93**, 1314–1318; (*c*) A. Sekiguchi, T. Matsuo and H. Watanabe, *J. Am. Chem. Soc.*, 2000, **122**, 5652–5653.

7 (*a*) D. Jędrzkiewicz, M. Morasch, O. P. E. Townrow, B. Rösch, J. Langer, Z. Mathe and S. Harder, *Chem. Sci.*, 2025, **16**, 17793–17802; (*b*) Y. Wang, R. Sun, J. Liang, Y. Zhang, B. Tan, C. Deng, Y.-H. Wang, B.-W. Wang, S. Gao and W. Huang, *J. Am. Chem. Soc.*, 2025, **147**, 7741–7748; (*c*) F. Delano IV and S. Demir, *Angew. Chem., Int. Ed.*, 2025, **64**, e202417217; (*d*) C. A. Gould, J. Marbey, V. Vieru, D. A. Marchiori, R. D. Britt, L. F. Chibotaru, S. Hill and J. R. Long, *Nat. Chem.*, 2021, **13**, 1001–1005; (*e*) P. L. Arnold, S. M. Mansell, L. Maron and D. McKay, *Nat. Chem.*, 2012, **4**, 668–674; (*f*) P. L. Diaconescu, P. L. Arnold, T. A. Baker, D. J. Mindiola and C. C. Cummins, *J. Am. Chem. Soc.*, 2000, **122**, 6108–6109.

8 (*a*) M. Liu, Y.-C. Chen, A. Mondal, H. Wang, M.-L. Tong, R. A. Layfield and F.-S. Guo, *J. Am. Chem. Soc.*, 2025, **147**, 11359–11367; (*b*) K. R. McClain, A. H. Vincent, A. Rajabi, D. X. Ngo, K. R. Meihaus, F. Furche, B. G. Harvey and J. R. Long, *J. Am. Chem. Soc.*, 2024, **146**, 32708–32716; (*c*) Y. Wang, Y. Zhang, J. Liang, B. Tan, C. Deng and W. Huang, *Chem. Sci.*, 2024, **15**, 10669; (*d*) W. Huang, F. Dulong, T. Wu, S. I. Khan, J. T. Miller, T. Cantat and P. L. Diaconescu, *Nat. Commun.*, 2013, **4**, 1448; (*e*) S. Krieck, H. Görls, L. Yu, M. Reiher and M. Westerhausen, *J. Am. Chem. Soc.*, 2009, **131**, 2977–2985.

9 (*a*) M. S. Hill, M. F. Mahon, A. S. S. Wilson, C. Dinoi, L. Maron and E. Richards, *Chem. Commun.*, 2019, **55**, 5732–5735; (*b*) P. L. Diaconescu and C. C. Cummins, *J. Am. Chem. Soc.*, 2002, **124**, 7660–7661; (*c*) H. Schumann, J. Winterfeld, L. Esser and G. Kociok-Köhn, *Angew Chem. Int. Ed. Engl.*, 1993, **32**, 1209–1210.

10 S. T. Liddle, *Coord. Chem. Rev.*, 2015, **293–294**, 211–227.

11 V. Beck and D. O'Hare, *J. Organomet. Chem.*, 2004, **689**, 3920–3938.

12 (*a*) T. L. Gianetti, G. Nocton, S. G. Minasian, N. C. Tomson, A. L. D. Kilcoyne, S. A. Kozimor, D. K. Shuh, T. Tyliszczak, R. G. Bergman and J. Arnold, *J. Am. Chem. Soc.*, 2013, **135**, 3224–3236; (*b*) Y.-C. Tsai, P.-Y. Wang, S.-A. Chen and J.-M. Chen, *J. Am. Chem. Soc.*, 2007, **129**, 8066–8067; (*c*) W. H. Monillas, G. P. A. Yap and K. H. Theopold, *Angew. Chem., Int. Ed.*, 2007, **46**, 6692–6694; (*d*) Y.-C. Tsai, P.-Y. Wang, K.-M. Lin, S.-A. Chen and J.-M. Chen, *Chem. Commun.*, 2008, 205–207.

13 Y.-S. Huang, G.-T. Huang, Y.-L. Liu, J.-S. K. Yu and Y.-C. Tsai, *Angew. Chem., Int. Ed.*, 2017, **56**, 15427–15431.

14 C. Ni, B. D. Ellis, J. C. Fettinger, G. J. Long and P. P. Power, *Chem. Commun.*, 2008, 1014–1016.

15 (*a*) G. C. Bazan, W. D. Cotter, Z. J. A. Komon, R. A. Lee and R. J. Lachicotte, *J. Am. Chem. Soc.*, 2000, **122**, 1371–1380; (*b*) G. E. Herberich and D. Söhnen, *J. Organomet. Chem.*, 1983, **254**, 143–147; (*c*) D. W. Clack and K. D. Warren, *Inorg. Chem.*, 1979, **18**, 513–519.

16 (*a*) R. Wang, C.-S. Lee and Z. Lu, *J. Organomet. Chem.*, 2023, **984**, 122564; (*b*) K. Rojales, M. Tamizmani, T. A. Bartholome and C. D. Martin, *Dalton Trans.*, 2022, **51**, 17216–17223; (*c*) J. He, F. Rauch, M. Finze and T. B. Marder, *Chem. Sci.*, 2021, **12**, 128–147; (*d*) S. K. Mellerup and S. Wang, *Trends Chem.*, 2019, **1**, 77–89; (*e*) E. von Grotthuss, A. John, T. Kaese and M. Wagner, *Asian J. Org. Chem.*, 2018, **7**, 37–53.

17 (*a*) P. Cui and Y. Chen, *Coord. Chem. Rev.*, 2016, **314**, 2–13; (*b*) A. J. Ashe, III, *Organometallics*, 2009, **28**, 4236–4248; (*c*) G. C. Fu, *Adv. Organomet. Chem.*, 2001, **47**, 101–119; (*d*) G. E. Herberich and H. Ohst, *Adv. Organomet. Chem.*, 1986, **25**, 199–236.

18 V. Pérez, S. S. Barnes and F.-G. Fontaine, *Eur. J. Inorg. Chem.*, 2014, 5698–5702.

19 G. E. Herberich, J. Hengesbach, G. Huttner, A. Frank and U. Schubert, *J. Organomet. Chem.*, 1983, **246**, 141–149.

20 (*a*) T. Heitkemper, J. Sarcevic and C. P. Sindlinger, *J. Am. Chem. Soc.*, 2020, **142**, 21304–21309; (*b*) G. E. Herberich, I. Hausmann, B. Hessner and M. Negele, *J. Organomet. Chem.*, 1989, **362**, 259–264.
21 J. Böhnke, H. Braunschweig, J. O. C. Jiménez-Halla, I. Krummenacher and T. E. Stennett, *J. Am. Chem. Soc.*, 2018, **140**, 848–853.
22 M. Dietz, M. Arrowsmith, S. Reichl, L. I. Lugo-Fuentes, J. O. C. Jiménez-Halla, M. Scheer and H. Braunschweig, *Angew. Chem., Int. Ed.*, 2022, **61**, e202206840.
23 M. Dietz, M. Arrowsmith, L. Endres, V. Paprocki, B. Engels and H. Braunschweig, *J. Am. Chem. Soc.*, 2023, **145**, 22222–22231.
24 T. Zhao, Y. Dai, P. Cui, C.-H. Tung and L. Kong, *J. Am. Chem. Soc.*, 2025, **147**, 40113–40119.
25 M. Dietz, M. Arrowsmith and H. Braunschweig, *Dalton Trans.*, 2024, **53**, 449–453.
26 (*a*) A. Lorbach, M. Bolte, H.-W. Lerner and M. Wagner, *Organometallics*, 2010, **29**, 5762–5765; (*b*) C. Balzereit, H.-J. Winkler, W. Massa and A. Berndt, *Angew Chem. Int. Ed. Engl.*, 1994, **33**, 2306–2308; (*c*) G. E. Herberich, B. Hessner and M. Hostalek, *Angew Chem. Int. Ed. Engl.*, 1986, **25**, 642–643.
27 (*a*) M. Tamizmani, J. R. Tidwell, E. W. Reinheimer, B. M. Lindley and C. D. Martin, *Inorg. Chem.*, 2023, **62**, 7150–7154; (*b*) C. Uhlmann, L. Münzfeld, A. Hauser, T.-T. Ruan, S. Kumar Kuppusamy, C. Jin, M. Ruben, K. Fink, E. Moreno-Pineda and P. W. Roesky, *Angew. Chem., Int. Ed.*, 2024, **63**, e202401372; (*c*) G. E. Herberich and B. Heßner, *Chem. Ber.*, 1982, **115**, 3115–3127.
28 P. Müller, S. Hucka, H. Köppel, H. Pritzkowa and W. Siebert, *Z. Naturforsch.*, 1995, **50b**, 1476–1484.
29 E. Januszewski, A. Lorbach, R. Grewal, M. Bolte, J. W. Bats, H.-W. Lerner and M. Wagner, *Chem. Eur J.*, 2011, **17**, 12696–12705.
30 E. von Grotthuss, S. E. Prey, M. Bolte, H.-W. Lerner and M. Wagner, *Angew. Chem., Int. Ed.*, 2018, **57**, 16491–16495.
31 P. Müller, B. Gangnus, H. Pritzkow, H. Schulz, M. Stephan and W. Siebert, *J. Organomet. Chem.*, 1995, **487**, 235–243.
32 (*a*) H. Schulz, H. Pritzkow and W. Siebert, *Chem. Ber.*, 1991, **124**, 2203–2207; (*b*) P. Müller, H. Pritzkow and W. Siebert, *J. Organomet. Chem.*, 1996, **524**, 42–47.
33 B. E. Mann, *Chem. Commun.*, 1971, 976–977.
34 R. D. Fischer, *Chem. Ber.*, 1960, **93**, 165–175.
35 F. Hanic and O. S. Mills, *J. Organomet. Chem.*, 1968, **11**, 151–158.
36 M. Trömel, *Z. Naturforsch.*, 2000, **55b**, 243–247.
37 (*a*) M. F. Bailey and L. F. Dahl, *Inorg. Chem.*, 1965, **4**, 1314–1319; (*b*) H.-B. Bürgi, A. Raselli, D. Braga and F. Grepioni, *Acta Crystallogr., Sect. B:Struct. Sci.*, 1992, **48**, 428–437; (*c*) J. M. Oh, S. J. Geib and N. J. Cooper, *Acta Crystallogr., Sect. C: Cryst. Struct. Commun.*, 1998, **54**, 581–583.
38 (*a*) E. von Grotthuss, M. Diefenbach, M. Bolte, H.-W. Lerner, M. C. Holthausen and M. Wagner, *Angew. Chem., Int. Ed.*, 2016, **55**, 14067–14071; (*b*) E. von Grotthuss, S. E. Prey, M. Bolte, H.-W. Lerner and M. Wagner, *J. Am. Chem. Soc.*, 2019, **141**, 6082–6091.
39 (*a*) Z. Chen, C. S. Wannere, C. Corminboeuf, R. Puchta and P. von Ragué Schleyer, *Chem. Rev.*, 2005, **105**, 3842–3888; (*b*) A. Stanger, *J. Org. Chem.*, 2006, **71**, 883–893.
40 C. Hoffend, M. Diefenbach, E. Januszewski, M. Bolte, H.-W. Lerner, M. C. Holthausen and M. Wagner, *Dalton Trans.*, 2013, **42**, 13826–13837.
41 K. B. Wiberg, *Tetrahedron*, 1968, **24**, 1083–1096.
42 A. E. Reed, R. B. Weinstock and F. Weinhold, *J. Chem. Phys.*, 1985, **83**, 735–746.
43 G. Knizia, *J. Chem. Theory Comput.*, 2013, **9**, 4834–4843.
44 R. F. W. Bader, *International Series of Monographs on Chemistry*, Oxford University Press: Oxford, UK, 1990, Vol. 22.
45 (*a*) CCDC 2538786: Experimental Crystal Structure Determination, 2026, DOI: 10.5517/ccdc.csd.cc2r6tb4; (*b*) CCDC 2538787: Experimental Crystal Structure Determination, 2026, DOI: 10.5517/ccdc.csd.cc2r6tc5; (*c*) CCDC 2538788: Experimental Crystal Structure Determination, 2026, DOI: 10.5517/ccdc.csd.cc2r6td6; (*d*) CCDC 2538789: Experimental Crystal Structure Determination, 2026, DOI: 10.5517/ccdc.csd.cc2r6tf7; (*e*) CCDC 2538790: Experimental Crystal Structure Determination, 2026, DOI: 10.5517/ccdc.csd.cc2r6tg8; (*f*) CCDC 2538791: Experimental Crystal Structure Determination, 2026, DOI: 10.5517/ccdc.csd.cc2r6th9; (*g*) CCDC 2538792: Experimental Crystal Structure Determination, 2026, DOI: 10.5517/ccdc.csd.cc2r6tjb; (*h*) CCDC 2538793: Experimental Crystal Structure Determination, 2026, DOI: 10.5517/ccdc.csd.cc2r6tkc; (*i*) CCDC 2538794: Experimental Crystal Structure Determination, 2026, DOI: 10.5517/ccdc.csd.cc2r6tld.